Increasing precision of lifetime determination in fluorescence lifetime imaging

Ching-Wei Chang[a] and Mary-Ann Mycek[a,b]

[a]Department of Biomedical Engineering, University of Michigan, Ann Arbor, MI, USA
[b]Applied Physics Program, University of Michigan, Ann Arbor, MI, USA

ABSTRACT

The interest in fluorescence lifetime imaging microscopy (FLIM) is increasing, as commercial FLIM modules become available for confocal and multi-photon microscopy. In biological FLIM applications, low fluorescence signals from samples can be a challenge, and this causes poor precision in lifetime. In this study, for the first time, we applied wavelet-based denoising methods in time-domain FLIM, and compared them with our previously developed total variation (TV) denoising methods. They were first tested using artificial FLIM images. We then applied them to low-light live-cell images. The results demonstrated that our TV methods could improve lifetime precision multi-fold in FLIM images and preserve the overall lifetime and pre-exponential term values when improving local lifetime fitting, while wavelet-based methods were faster. The results here can enhance the precision of FLIM, especially for low-light and / or fast video-rate imaging, to improve current and rapidly emerging new applications of FLIM such as live-cell, *in vivo* whole-animal, or endoscopic imaging.

Keywords: Time-gated FLIM, precision improvement, denoising, wavelet analysis, total variation

1. INTRODUCTION

Fluorescence lifetime imaging and fluorescence lifetime imaging microscopy (FLIM) are useful molecular imaging techniques for pre-clinical and clinical studies in living cells, tissues, small animals, and endoscopic samples, with fluorescence lifetime serving as the image contrast [1]. It can be used as optical sensors to indicate micro-environmental conditions such as oxygen levels, the state of endogenous / exogenous fluorophores, and Förster resonance energy transfer in live cells [2-5]. The interest in FLIM is increasing, as commercial FLIM modules become available for confocal and multi-photon microscopy.

However, in biological FLIM applications, low fluorescence signals from samples can be a challenge, and this causes poor precision in lifetime. To improve the precision of lifetime determination, optimal gating can be implemented for time-gated FLIM [6]. Alternatively, image "denoising" (noise removal) also improves the precision of fluorescence images [7-9].

In this study, therefore, for the first time, we evaluate the applications of wavelet-based denoising methods on time-domain FLIM to improve lifetime precision, and compared them with our previously developed total variation (TV) denoising methods [6] in this particular application.

2. METHODS

2.1 Time-gated FLIM system

To implement time-gated FLIM, we have designed and characterized a novel wide-field, time-domain FLIM system developed for picosecond time-resolved biological imaging [5, 10, 11]. A nitrogen laser is used to pump a dye laser for UV-visible-NIR excitation, offering a significantly less expensive, wide-field, and potentially portable / clinically applicable alternative to multi-photon excitation for sub-nanosecond FLIM imaging of biological samples [11]. The large temporal dynamic range of 750 ps – 1 μs, the lifetime discrimination of 50 ps, and the 1.4 μm spatial resolution of the system make it suitable for studying many biological endogenous and exogenous fluorophores [12-14]. To create fluorescence

Three-Dimensional and Multidimensional Microscopy: Image Acquisition and Processing XVII, edited by Jose-Angel Conchello, Carol J. Cogswell, Tony Wilson, Thomas G. Brown, Proc. of SPIE Vol. 7570, 757007

lifetime maps rapidly with acceptable precision, a four-gate protocol with an analytical least squares lifetime determination algorithm was used on a pixel-by-pixel basis. It is more precise than the two-gate protocol while still easy to handle [15-17].

2.2 Optimal gating

Optimal gating parameters *g* (gate width) and *dt* (time interval between two consecutive gates) were determined previously with Monte Carlo simulations [18]. The Monte Carlo simulation procedure was similar to the one used for the accuracy and precision estimation of the denoising methods (section 2.5), except that different *g* and *dt* values were used in individual simulations without performing any image denoising. This could also be regarded as using one single pixel in the undenoised case with varying gating parameters. Optimal *g* and *dt* were found to achieve the best precision of lifetime determination. The optimal gating scheme of the artificial images (section 2.4) was determined to be $g = 16$ and $dt = 4$. It was an optimal gating scheme for a certain lifetime range in which our lifetime setting was covered.

2.3 Denoising methods

The first wavelet-based denoising method employed in this study utilized basic, unmodified Discrete Wavelet Transform (DWT). Image denoising was implemented with four levels of decomposition and soft-thresholding using Matlab's Wavelet Toolbox version 4.4. The default threshold determination method for wavelet denoising (using universal thresholding and median absolute value of the detail coefficients) was not used due to the fact that its estimated noise level was zero and hence no denoising would be performed for our artificial images (described in section 2.4) corrupted by Poisson noise. Therefore, the threshold values were determined by using mean absolute value. Global thresholding was used for each gated image. The wavelet biorthogonal 3.7 (bior 3.7) was chosen, not only because it is a commonly used wavelet but also because it has been demonstrated to perform well in frequency-domain FLIM for background subtraction and denoising [8].

A more sophisticated wavelet-based algorithm developed by Willet et al. [19, 20] and employed in this study (denoted as "Poisson Wavelet" below) is a Bayesian approach to Poisson intensity estimation based on the translation invariant (TI) hereditary unnormalized Haar wavelet transform. This type of wavelets allows a simple formulation in the case of Poisson data.

The wavelet methods were compared with our previously developed TV models [18]. The first one was the *f*-weighted TV (FWTV) that can deal with Poisson-distributed noise, and the other one was a modified version of FWTV for handling non-Poisson noise (such as a combination of different forms of noise at low photon counts with real imaging systems).

2.4 Artificial images

Because artificial images have predetermined parameters, we employed them to evaluate the accuracy and precision of the denoising algorithms. The fluorescence decay model used in this study was single-exponential with the intensity profile $I(t) = \alpha \exp(-t/\tau)$, where τ is fluorescence lifetime and α is a pre-exponential term.

The geometry that we may encounter with live-cell FLIM was mimicked in our artificial images. It consisted of "the ring" (the large open circle shown in the right panel of Figure 1) with $\tau = 5$ and $\alpha = 1000$, "the inner circle" (the centered solid circle inside the ring) with $\tau = 10$ and $\alpha = 1000$, and "the satellite" (the small dot to the bottom right of the inner circle and the ring) with $\tau = 10$ and $\alpha = 50$. The image size was 128 pixels × 128 pixels.

2.5 Monte Carlo simulations

Monte Carlo simulations were used, along with the artificial images and the predetermined lifetime values (section 2.4), to construct the distribution of lifetime determined from Poisson-noise-corrupted intensity images for each pixel, either with or without denoising. Denoising, if implemented, was performed on each gated intensity images before lifetime map construction. The number of simulations was 20 in each denoised or undenoised case.

2.6 Estimation of accuracy and precision

After all lifetime values from the MC simulations were collected, the mean and the standard deviation of the lifetime values from all the MC simulations were calculated, and these values were used for the evaluation of accuracy and precision with RSD (relative standard deviation) and RME (relative mean error). RSD (%) was defined as [standard deviation / mean value] × 100. RME (%), on the other hand, was defined as [(mean value – correct value) / correct value] × 100.

2.7 Live-cell sample preparation

BCECF, AM (Invitrogen, CA), was used to stain live HCT-116 cells (purchased from ATCC). After the confluence of the cells reached about 80% in culture dishes, the culture media were removed and phosphate buffered saline (PBS) was used to wash the dishes three times. The cells were then incubated at 37°C with 1μM BCECF, AM, in PBS for one hour before using the FLIM system for imaging. The gating parameters were dt = 1 ns and g = 0.2 ns, which were not the optimal gating scheme; this was to better evaluate the ability of the denoising methods to handle images with low SNR (signal-to-noise ratio). For each FLIM gating, five images were used for averaging.

3. RESULTS

3.1 Artificial images

The performance of precision improvement was method- and geometry-dependent; FWTV and Poisson Wavelet performed equally well with the ring being most difficult to denoise. The results are illustrated in Figure 1, where the RSD value at each pixel is shown for the lifetime map constructed with either undenoised or denoised artificial intensity images using two different denoising methods. In the undenoised image, apparently the satellite had a much higher RSD value due to its much lower total photon counts (TC, = $\alpha\tau$). Note that in the artificial images TC was kept relatively high, compared to the live-cell imaging (section 3.2), for better characterization. After denoising with the three methods (FWTV [18], DWT, and Poisson Wavelet), all the three objects had their RSD values lowered and the precision improvement was most significant in the inner circle. We could clearly observe that DWT had the worst effect and FWTV was the best (data not shown, precision improvement was multi-fold when compared with the undenoised case), with Poisson Wavelet slightly worse than FWTV. The ring was most difficult to denoise for all the three methods. This was probably due to the fact that the ring had an edge-rich geometry. Interestingly, for the satellite, DWT produced the best precision, but it had issues regarding the accuracy that will be described below.

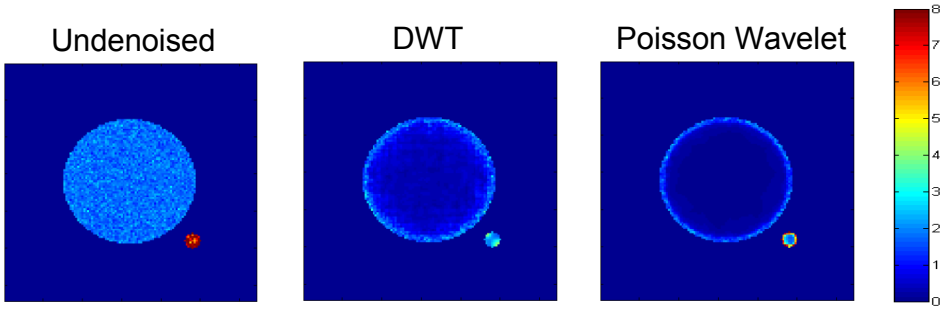

Figure 1. RSD (relative standard deviation), indicating the precision, of the lifetime map constructed with the undenoised and denoised artificial images using two different denoising methods.

Both FWTV and Poisson Wavelet preserved the accuracy of lifetime determination after denoising. Figure 2 illustrates the RME values, which indicate the accuracy. As we can expect, in the undenoised image, since the noise was defined by Poisson random distribution, the accuracy of lifetime determination should be minimally affected, and this image therefore should serve as the standard accuracy the denoising methods should be aimed at. After FWTV [18] and Poisson Wavelet denoising, the accuracy was mostly preserved relative to the undenoised case, with Poisson Wavelet method slightly better especially for the satellite. On the other hand, DWT denoising suffered from severe inaccuracy for the ring and the satellite and even for the inner circle (lower RME on the edge but higher RME off the edge).

As for the running times for each 128 × 128 image, DWT was the fastest and Poisson Wavelet was slightly slower, with FWTV being the slowest.

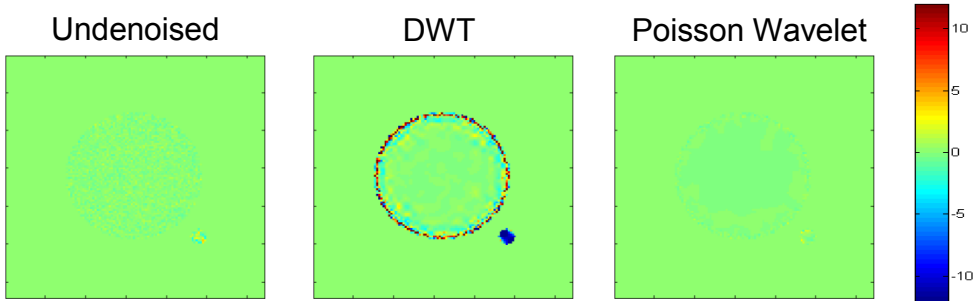

Figure 2. RME (relative mean error), indicating the accuracy, of the lifetime map constructed with the undenoised and denoised artificial images using two different denoising methods.

3.2 Live-cell FLIM

To demonstrate that the denoising methods can be applied to live-cell images acquired from real FLIM systems, FWTV, Poisson Wavelet, and a modified FWTV were used to denoise the gated fluorescence intensity images before lifetime map construction. DWT was not used since it suffered from severe inaccuracy (section 3.1). The modified FWTV was used since real image systems, especially at low photon counts, have forms of noise other than Poisson distribution. Optimal gating was not implemented in this case for better evaluation of the ability of the denoising methods to handle images with low SNR. The total photon counts were around 600 only.

For live-cell images acquired with the FLIM system, the modified FWTV best preserved the overall τ and α values while improving local lifetime fitting. If FWTV was not modified, the intensity images could be over-smoothened and the lifetime value would be inaccurate. Similar phenomenon happened to Poisson Wavelet denoising as well, presumably due to the fact that the assumption of noise distribution was not appropriate for low-light live-cell imaging. The lifetime values, after averaging, were then compared with the averaged undenoised lifetime value, which should remain almost constant pre- and post-denoising, due to the randomness of the uncertainties. Our results clearly demonstrated that the modified FWTV could best preserve the overall τ and α values while still removing uncertainties and improving local lifetime fitting.

4. CONCLUSIONS AND FUTURE WORK

In this study, TV-based and wavelet-based image denoising methods were characterized for individual strengths and weaknesses with artificial images and live-cell images acquired from a real FLIM system. With artificial images, FWTV and Poisson Wavelet performed almost equally well (multi-fold precision improvement, depending on the geometry of objects) and better than DWT in terms of both precision and accuracy, with DWT and Poisson Wavelet running faster. For live-cell images acquired with the FLIM system, the modified FWTV best preserved the overall τ and α values while still improving local lifetime fitting.

The results here can enhance the precision of FLIM, especially for low-light and / or fast video-rate imaging, to improve current and rapidly emerging new applications of FLIM such as live-cell, *in vivo* whole-animal, or endoscopic imaging.

Future work includes investigating a more sophisticated approach to threshold determination of, and using local thresholding in, DWT and other wavelet-based methods for FLIM use. Also, high-speed FWTV can be developed by improving the code efficiency and adopting advanced algorithms, such as the ones developed by Chambolle [21] and Figueiredo *et al.* [22]. Finally, since precise and accurate noise removal can improve other advanced image processing techniques such as image deconvolution [23], segmentation, and object tracking, the combination of denoising and these techniques will be studied for FLIM use as well.

ACKNOWLEDGMENTS

This work was supported in part by National Institutes of Health grant R01-CA-114542 (to M.-A.M.).

REFERENCES

[1] C. W. Chang, D. Sud and M. A. Mycek, "Fluorescence lifetime imaging microscopy," Methods Cell Biol 81 495-524 (2007)

[2] C. W. Chang, M. Wu, S. D. Merajver and M. A. Mycek, "Physiological fluorescence lifetime imaging microscopy improves Förster resonance energy transfer detection in living cells," Journal of Biomedical Optics 14(6), 060502 (2009)

[3] D. Sud, G. Mehta, K. Mehta, J. Linderman, S. Takayama and M. A. Mycek, "Optical imaging in microfluidic bioreactors enables oxygen monitoring for continuous cell culture," Journal of Biomedical Optics 11(5), 050504 (2006)

[4] D. Sud and M. A. Mycek, "Calibration and validation of an optical sensor for intracellular oxygen measurements," Journal of Biomedical Optics 14(2), 020506 (2009)

[5] D. Sud, W. Zhong, D. G. Beer and M. A. Mycek, "Time-resolved optical imaging provides a molecular snapshot of altered metabolic function in living human cancer cell models," Optics Express 14(10), 4412-4426 (2006)

[6] C. W. Chang and M. A. Mycek, "Improving precision in time-gated FLIM for low-light live-cell imaging," Proc. SPIE 7370 7370091-7370096 (2009)

[7] C. Vonesch, "Fast and automated wavelet-regularized image restoration in fluorescence microscopy," Ph.D. thesis, École Polytechnique Fédérale De Lausanne (2009)

[8] C. Buranachai, D. Kamiyama, A. Chiba, B. D. Williams and R. M. Clegg, "Rapid frequency-domain FLIM spinning disk confocal microscope: Lifetime resolution, image improvement and wavelet analysis," Journal of Fluorescence 18(5), 929-942 (2008)

[9] A. Buades, B. Coll and J. M. Morel, "A review of image denoising algorithms, with a new one," Multiscale Modeling & Simulation 4(2), 490-530 (2005)

[10] W. Zhong, M. Wu, C. W. Chang, K. A. Merrick, S. D. Merajver and M. A. Mycek, "Picosecond-resolution fluorescence lifetime imaging microscopy: a useful tool for sensing molecular interactions in vivo via FRET," Optics Express 15(26), 18220-18235 (2007)

[11] P. Urayama, W. Zhong, J. A. Beamish, F. K. Minn, R. D. Sloboda, K. H. Dragnev, E. Dmitrovsky and M. A. Mycek, "A UV-visible-NIR fluorescence lifetime imaging microscope for laser-based biological sensing with picosecond resolution," Applied Physics B-Lasers and Optics 76(5), 483-496 (2003)

[12] P. K. Urayama, J. A. Beamish, F. K. Minn, E. A. Hamon and M.-A. Mycek, "A UV fluorescence lifetime imaging microscope to probe endogenous cellular fluorescence," in Conference on Lasers and Electro-Optics, pp. 550-551, Optical Society of America, Washington D.C. (2002).

[13] P. K. Urayama and M. A. Mycek, "Fluorescence lifetime imaging microscopy of endogenous biological fluorescence," in Handbook of Biomedical Fluorescence M. A. Mycek and B. W. Pogue, Eds., Marcel Dekker, Inc., New York (2003).

[14] W. Zhong, P. Urayama and M.-A. Mycek, "Imaging fluorescence lifetime modulation of a ruthenium-based dye in living cells: the potential for oxygen sensing," Journal of Physics D: Applied Physics 36(14), 1689-1695 (2003)

[15] I. Bugiel, K. König and H. Wabnitz, "Investigation of cell by fluorescence laser scanning microscopy with subnanosecond time resolution," Lasers in the Life Sciences 3(1), 47-53 (1989)

[16] X. F. Wang, T. Uchida, D. M. Coleman and S. Minami, "A two-dimensional fluorescence lifetime imaging system using a gated image intensifier," Appl Spectrosc 45(3), 360-366 (1991)

[17] K. K. Sharman, A. Periasamy, H. Ashworth, J. N. Demas and N. H. Snow, "Error analysis of the rapid lifetime determination method for double-exponential decays and new windowing schemes," Anal Chem 71(5), 947-952 (1999)

[18] C. W. Chang, "Improving Accuracy and Precision in Biological Applications of Fluorescence Lifetime Imaging Microscopy," Ph.D. thesis, University of Michigan (2009)

[19] R. M. Willett and R. D. Nowak, "Fast multiresolution photon-limited image reconstruction," 2004 2nd Ieee International Symposium on Biomedical Imaging: Macro to Nano, Vols 1 and 2 1192-1195 (2004)

[20] I. Rodrigues, J. Sanches and J. Bioucas-Dias, "Denoising of Medical Images Corrupted by Poisson Noise," 2008 15th Ieee International Conference on Image Processing, Vols 1-5 1756-1759 (2008)

[21] A. Chambolle, "Total variation minimization and a class of binary MRF models," Energy Minimization Methods in Computer Vision and Pattern Recognition, Proceedings 3757(136-152 (2005)
[22] M. A. T. Figueiredo, J. B. Dias, J. P. Oliveira and R. D. Nowak, "On total variation denoising: A new majorization-minimization algorithm and an experimental comparison with wavalet denoising," Proceedings International Conference on Image Processing, Vols 1-7 2633-2636 (2006)
[23] D. Sud and M. A. Mycek, "Image restoration for fluorescence lifetime imaging microscopy (FLIM)," Optics Express 16(23), 19192-19200 (2008)